Three-band MRI Image Fusion Utilizing the Wavelet-based Method Optimized with Two Quantitative Fusion Metrics

Yufeng Zheng, Adel S Elmaghraby and Hichem Frigui

Dept. of Computer Engineering and Computer Science, University of Louisville (USA)

ABSTRACT

In magnetic resonance imaging (MRI), there are three bands of images ("MRI triplet") available, which are T1-, T2- and PD-weighted images. The three images of a MRI triplet provide complementary structure information and therefore it is useful for diagnosis and subsequent analysis to combine three-band images into one. We propose an advanced discrete wavelet transform (*a*DWT) for three-band MRI image fusion and the *a*DWT algorithm is further optimized utilizing two quantitative fusion metrics – the image quality index (IQI) and ratio spatial frequency error (rSFe). In the *a*DWT method, principle component analysis (PCA) and morphological processing are incorporated into a regular DWT fusion algorithm. Furthermore, the *a*DWT has two adjustable parameters – the level of DWT decomposition (L_d) and the length of the selected wavelet (L_w) that determinately affect the fusion result. The fused image quality can be quantitatively measured with the established metrics – IQI and rSFe. Varying the control parameters (L_d and L_w), an iterative fusion procedure can be implemented and running until an optimized fusion is achieved. We fused and analyzed several MRI triplets from the Visible Human Project® female dataset. From the quantitative and qualitative evaluations of fused images, we found that (1) the *a*DWTi-IQI algorithm produces a smoothed image whereas the *a*DWTi-rSFe algorithm yields a sharpened image, (2) fused image "T1+T2" is the most informative one in comparison with other two-in-one fusions (PD+T1 and PD+T2), (3) for three-in-one fusions, no significant difference is observed among the three fusions of (PD+T1)+T2, (PD+T2)+T1 and (T1+T2)+PD, thus the order of fusion does not play an important role. The fused images can significantly benefit medical diagnosis and also the further image processing such as multi-modality image fusion (with CT images), visualization (colorization), segmentation, classification and computer-aided diagnosis (CAD).

Keywords: Magnetic Resonance Imaging, Image fusion, Iterative fusion, Discrete wavelet transform (DWT), Fusion evaluation, Image quality index, Spatial frequency.

1. INTRODUCTION

Image fusion combines multiple-source imagery by using advanced image processing techniques. Specifically, it integrates disparate or complementary images in order to enhance the information apparent in the respective source images, as well as to increase the reliability of interpretation. This leads to more accurate image[1] and increased confidence (thus reduced ambiguity), and improved classification.[2-4] This paper focuses on the "pixel-level" fusion process, where a composite image has to be built of two or more input images. A general framework of image fusion can be found elsewhere.[5] In image fusion, some general requirements,[6] for instance, pattern conservation and distortion minimization, need to be followed. To measure the image quality, the quantitative evaluation of fused imagery has to be considered such that an objective comparison of the performance of different fusion algorithms can be carried out. In addition, a quantitative measurement may potentially be used as a feedback to the fusion algorithm to further improve the fused image quality.

Through the wide applications of image fusion in medical imaging, remote sensing, nighttime operations and multi-spectral imaging, many fusion algorithms have been developed. Two common fusion methods are the discrete wavelet transform (DWT)[6-10] and various pyramids (such as Laplacian, contrast, gradient and morphological pyramids).[11-21] As with any pyramid method, the wavelet-based fusion method is also a multi-scale analysis method. The studies[22-24] showed that the DWT method has more complete theoretical support as well as further development potentials. For example, Ref. [22] showed that an advanced DWT (*a*DWT) fusion algorithm is superior to any pyramid-based method,

Medical Imaging 2006: Image Processing, edited by Joseph M. Reinhardt, Josien P. W. Pluim,
Proc. of SPIE Vol. 6144, 61440R, (2006) · 0277-786X/06/$15 · doi: 10.1117/12.651689

and Refs. [23-34] presented an iterative *a*DWT (*a*DWTi) algorithm optimized by a given fusion metric. This paper will discuss the iterative *a*DWT method and its applications to MRI image fusion.

Magnetic resonance imaging (MRI) can create internal images of the soft tissues of the body using combinations of radio waves and magnetic fields. Three bands of MRI images (referred as a "MRI triplet") are available in MRI imaging, i.e., T1-, T2- and PD-weighted images, where T1 (spin lattice relaxation) and T2 (spin spin relaxation) are the time constants corresponding to the imaging tissues, PD (proton density) reflects the number of hydrogen atoms in the imaging region. The three images of a MRI triplet provide complementary structure information and therefore it is useful for diagnosis and subsequent analysis to combine (i.e., fuse) three weighted images into one. Aguilar[25-26] et. al. proposed to fuse and then colorize medical images with a neural network-based fusion architecture. Hereby we aim at how to optimize then improve the fused image quality under the wavelet-based fusion framework. Specifically, to improve the fused image quality in MRI image fusion, we propose to use the iterative *a*DWT algorithms that are optimized utilizing two fusion metrics – the image quality index (IQI)[23] and ratio spatial frequency error (rSFe).[24] The *spatial frequency* (SF) and *entropy* are also used to measure the image quality.

The subsequent sections of this paper are organized as follows. First, the image fusion metrics and methods are fully described. Then the experimental results and discussions are presented. Lastly conclusions are drawn based on the experimental analyses.

2. IMAGE FUSION METRICS AND METHODS

There are four image quality metrics and two wavelet-based fusion algorithms that are used in our MRI image fusion. We first discuss the fusion metrics and then introduce the DWT fusion methods.

2.1 Image quality metrics

As mentioned in the introduction, the general requirements of an image fusion process are that it should preserve all useful pattern information from the source images and meanwhile it should not introduce artifacts that could interfere with subsequent analyses.[27] However, it is nearly impossible to combine images without introducing some form of distortion. In this subsection we discuss quantitative (i.e., objective) measures (non-requisite for ground truths) that could be carried out automatically by computers.

2.1.1 Entropy

Entropy is given by the following equation

$$Entropy = -\sum_{l=0}^{L-1} p(l)\log_2 p(l)\,, \tag{1}$$

where $p(l)$ is the probability of gray level l, and the dynamic range of the analyzed image is [0, L-1] (typically L = 256).

2.1.2 Image quality index

The *image quality index* was recently introduced by Wang and Bovik.[28] Given two sequences $x = (x_1, \ldots, x_n)$ and $y = (y_1, \ldots, y_n)$, let $\bar{x}$ denote the mean of x, and σ_x and σ_{xy} denote the variance of x and covariance of x and y, respectively. The global quality index of two vectors is defined as

$$Q_0(x,y) = \frac{4\sigma_{xy}\bar{x}\bar{y}}{(\bar{x}^2+\bar{y}^2)(\sigma_x^2+\sigma_y^2)}\,, \tag{2}$$

which can be decomposed as

$$Q_0(x,y) = \frac{\sigma_{xy}}{\sigma_x\sigma_y}\cdot\frac{2\bar{x}\bar{y}}{(\bar{x}^2+\bar{y}^2)}\cdot\frac{2\sigma_x\sigma_y}{(\sigma_x^2+\sigma_y^2)}\,. \tag{3}$$

Note that the first component in Eq. (3) is the correlation coefficient between x and y. This value is a measure for the *similarity* of the vectors x and y, and takes values between 0 and 1 (considering the image quality evaluation where the values x_i, y_i are positive grayscale values). The second component in Eq. (3) corresponds to the *luminance distortion* which has a dynamic range of [0, 1]. The third factor in Eq. (3) measures the *contrast distortion* and its range is also [0, 1]. In summary, $Q_0 \in [0, 1]$, and the maximum value $Q_0 = 1$ is achieved when x and y are identical.

Piella and Heijmans[29] introduced a weighting procedure into Q_0 calculation. The weight should reflect the local relevance of an input image that may depend on its local variance, contrast, sharpness, or entropy. Given the local *salience* (e.g., local variance) of two input images A and B, we compute a local weight λ indicating the relative importance of image A compared to image B: the larger λ, the more weight is given to image A. A typical choice for λ is

$$\lambda = S(\mathrm{I_A}) / [S(\mathrm{I_A}) + S(\mathrm{I_B})], \tag{4}$$

where $S(\mathrm{I_A})$ and $S(\mathrm{I_B})$ denote the salience of input image A and B, respectively. Then, the weighted image quality index (IQI) can be defined as

$$Q_w = \lambda Q_0(\mathrm{I_A}, \mathrm{I_F}) + (1-\lambda)\, Q_0(\mathrm{I_B}, \mathrm{I_F}). \tag{5}$$

Since image signals are generally non-stationary, it is more appropriate to measure the weighted image quality index Q_w over local regions (e.g., by partitioning the entire image into a set of 'blocks') and then combine these local results into a single measure as the global measure of the entire image. Piella also suggested using local variance as the salience of an image, i.e., $S(\mathrm{I_A}) = \sigma_A$. In fact, the IQI metric measures the similarity between the fused image ($\mathrm{I_F}$) and both of the input images ($\mathrm{I_A}$ and $\mathrm{I_B}$) by assuming that an ideally fused image should resemble both original input images. For example, in our experiments, dividing each image ($\mathrm{I_A}$, $\mathrm{I_B}$ or $\mathrm{I_F}$) into a certain number of blocks by designating the block size of 16×16 pixels, compute each Q_0 on each small bock (window), then sum all Q_0's up through all blocks and finally take the average.

2.1.3 Spatial frequency

The metric "*spatial frequency*" (SF)[30-31] is used to measure the overall activity level of an image, which is defined as follows.

$$SF = \sqrt{(RF)^2 + (CF)^2}\,, \tag{6}$$

where *RF* and *CF* are row frequency and column frequency respectively.

$$RF = \sqrt{\frac{1}{MN}\sum_{i=1}^{M}\sum_{j=2}^{N}[I(i,j) - I(i,j-1)]^2}\,, \tag{7a}$$

$$CF = \sqrt{\frac{1}{MN}\sum_{j=1}^{N}\sum_{i=2}^{M}[I(i,j) - I(i-1,j)]^2}\,. \tag{7b}$$

Notice that the term of "spatial frequency" that is computed in spatial domain as defined in Eqs. (6-7), does not correspond with Fourier transform where the spatial frequency is measured in frequency domain with the unit of "cycles per degree" or "cycles per millimeter".

2.1.4 The ratio of SF error

Similar to the definitions of *RF* and *CF*, spatial frequency along two diagonal directions, termed as main diagonal SF (*MDF*) and secondary diagonal SF (*SDF*), can be defined as below,

$$MDF = \sqrt{w_d \cdot \frac{1}{MN}\sum_{i=2}^{M}\sum_{j=2}^{N}[I(i,j) - I(i-1,j-1)]^2}\,, \tag{8a}$$

$$SDF = \sqrt{w_d \cdot \frac{1}{MN}\sum_{j=1}^{N-1}\sum_{i=2}^{M}[I(i,j) - I(i-1,j+1)]^2}\,, \tag{8b}$$

where $w_d = 1/\sqrt{2}$ is a distance weight; similarly it can be considered that $w_d = 1$ in Eqs. (7).

Then the overall spatial frequency of an image becomes

$$SF = \sqrt{(RF)^2 + (CF)^2 + (MDF)^2 + (SDF)^2}\,, \tag{9}$$

which is a combination of four directional SFs.

With Eq. (9) we can calculate the SFs of input images ($\mathrm{SF_A}$ and $\mathrm{SF_B}$) and the SF of the fused image ($\mathrm{SF_F}$). Now we determine how to calculate a reference SF ($\mathrm{SF_R}$) with which the $\mathrm{SF_F}$ can be compared. The four *differences* (inside square brackets) defined in Eqs. (7-8) are actually the four first-order *gradients* along four directions at that pixel, denoted as *Grad*(I(i,j)). The four reference gradients can be obtained by taking the maximum of absolute gradient values

between input image A and B along four directions:

$$Grad^{D}(I_R(i,j)) = \max\{\text{abs}[Grad^{D}(I_A(i,j))], \text{abs}[Grad^{D}(I_B(i,j))]\},$$
$$\text{for each of four directions, i.e., } D = \{H, V, MD, SD\}, \quad (10)$$

where 'D' denotes one of four directions (Horizontal, Vertical, Main Diagonal, and Secondary Diagonal). Substituting the differences (defined inside square brackets) in Eqs. (7-8) with $Grad^{D}(I_R(i,j))$, four directional reference SFs (i.e., RF_R, CF_R, MDF_R and SDF_R) can be calculated. For example, the reference row frequency can be calculated as follows:

$$RF_R = \sqrt{\frac{1}{MN}\sum_{i=1}^{M}\sum_{j=2}^{N}[Grad^{H}(I_R(i,j))]^2} \ . \quad (11)$$

Similar to Eq. (9), the SF_R can be computed by combining four directional reference SFs. Note that the notation of "$Grad^{H}(I_R(i,j))$" is interpreted as "the horizontal reference gradient at point (i,j)", and no reference image is needed to compute the SF_R value.

Finally, the *ratio of SF error* (rSFe) is defined as follows:

$$\text{rSFe} = (SF_F - SF_R) / SF_R. \quad (12)$$

Obviously, an ideal fusion has rSFe = 0; that is, the smaller rSFe's absolute value, the better the fused image. Furthermore, rSFe > 0 means that an *over-fused* image, with some distortion or noise introduced, has resulted; rSFe < 0 denotes that an *under-fused* image, with some meaningful information lost, has been produced.

2.2 Image fusion methods

In this subsection, an advanced discrete wavelet transform (*a*DWT)[22] method that incorporates *principal component analysis* (PCA) and morphological processing into a regular DWT fusion algorithm is first reviewed. Two iterative fusion algorithms are then briefly described which are optimized by two established metrics – IQI[23] and rSFe,[24] respectively.

2.2.1 The advanced DWT method

The regular DWT method is a multi-scale analysis method. In a regular DWT fusion process, DWT coefficients from two input images' are fused pixel-by-pixel by choosing the average of the approximation coefficients at the highest transform scale; and the larger absolute value of the detail coefficients at each transform scale. Then an inverse DWT is performed to obtain the fused image. At each DWT scale of a particular image, the DWT coefficients of a 2D image consist of four parts: approximation, horizontal detail, vertical detail and diagonal detail. In the *advanced DWT* (*a*DWT) method, we apply PCA to the two input images' approximation coefficients at the highest transform scale, that is, we fuse them by using the *principal eigenvector* (corresponding to the larger *eigenvalue*) derived from the two 'original' images, as described in Eq. (13) below:

$$C_F = (a_1 \cdot C_A + a_2 \cdot C_B)/(a_1 + a_2), \quad (13)$$

where C_A and C_B are approximation coefficients transformed from input images A and B. C_F represents the fused coefficients; a_1 and a_2 are the elements of the principal eigenvector, which are computed by analyzing the 'original' input images (Note: not analyzing C_A and C_B because their sizes at the highest transform scale are too small to conduct an accurate result). Note that the denominator in Eq. (13) is used for normalization so that the fused image has the same energy distribution as the original input images.

In combining the detail coefficients (the other three quarters of the coefficients) at each transform scale, the larger absolute values are selected, followed by a neighborhood (e.g., a 3×3 window) morphological processing, which serves to verify the selected pixels by using a "filling" and "cleaning" operation (i.e., the operation fills or removes isolated pixels locally). For example, in a 3×3 processing window (sliding pixel-by-pixel over the whole image), if the central coefficient was selected from Image A but all its 8-surrounding coefficients were selected from Image B, then after the 'filling' process the central one would be replaced with the detail coefficient from Image B. Such an operation (similar to smoothing) can increase the consistency of coefficient selection thereby reducing the distortion in the fused image.

2.2.2 The iterative *a*DWT optimized by the IQI

The IQI value (discussed in Section 2.1.2) is calculated to measure the image quality fused by the *a*DWT, then it is fed back to the fusion algorithm in order to achieve a better fusion by adjusting parameters. Previous experiments[22] have pointed to an important relationship between the fused image quality and the wavelet properties, that is, a higher level DWT decomposition (with smaller image resolution at higher scale) or a lower order of wavelets (with shorter length)

Table 1: The SF and entropy values of three-band MRI images from six slices (refer to Figs. 1, 4, 7 and 10)

MRI Slice #	MRI_1104		MRI_1124		MRI_1134		MRI_4502		MRI_1154		MRI_4450	
Metric	SF	Entropy	SF	Entropy	SF	Entropy	SF	Entropy	SF	Entropy	SF	Entropy
PD	28.4835	5.7563	28.8492	5.7260	26.7923	5.6565	34.6461	7.1043	26.7980	5.6968	24.1026	6.7074
T1	27.1999	5.4611	27.6022	5.5154	30.1577	5.8635	36.7420	7.2133	26.4114	5.8740	29.4007	7.0510
T2	23.6816	5.5839	26.2818	5.7043	23.9474	5.4279	30.6362	6.8519	25.1200	5.7496	19.6315	6.1224

usually resulted in a more sharpened fused image. This means that we can use the level of DWT decomposition (Notated as L_d) and the length of a wavelet (notated as L_w) as adjusted parameters of an iterative *a*DWT (*a*DWTi) algorithm. If measured with the IQI, its value usually tends to be large for a fused image with a larger L_d or a larger L_w. The combination of the *a*DWTi algorithm and the IQI metric derives a new algorithm, termed as "*a*DWTi-IQI". With the definition of IQI, we know that it has an ideal value, 1, but it cannot give the *error direction* (i.e., positive or negative) because of $0 < IQI \leq 1$ (i.e., always IQI-1 < 0).

Of course, a termination condition is needed in order to stop the fusion iteration. The fusion iteration stops when (1) the IQI value converges at its ideal value, i.e., the absolute value of (IQI-1) is smaller than a designated tolerance error; (2) there is no significant change of the IQI values between two adjacent iterations; (3) the IQI value is generally decreasing for subsequent iterations; (4) the parameters' boundaries are reached. In implementing the iteration of a fusion procedure, appropriate boundaries of varying parameters should be designated based on the definition of parameters and the context. The details of implementation are depicted in Ref. [23].

2.2.3 The iterative *a*DWT optimized by the rSFe

The similar fusion procedure as depicted in Section 2.2.2 is applicable here except for the optimization metric. Hereby we use the rSFe metric to direct the iterative fusion process that results in another algorithm, "*a*DWTi-rSFe". Notice that the error of the rSFe value (subtracting the current rSFe value from the ideal value, 0) can indicate the *error direction* (positive or negative), which is useful to decide the parameters (L_d and L_w) adjustment (i.e., increment or decrement). For example, if the current rSFe(L_d, L_w) < 0, then increase L_d or decrease L_w for next *a*DWTi fusion process. One more termination condition is applicable to the *a*DWTi-rSFe algorithm, that is, stop the iteration when the rSFe value crosses over 'zero' (the ideal value). Taking the advantage of the sign of rSFe the iteration procedure can eventually be expedited.

3. EXPERIMENTS AND DISCUSSIONS

In our experiments, the MRI images were from the Visible Human Project® female dataset (Provided by the National Library of Medicine). The female dataset consists of axial MR images of the head and neck taken at 4 mm intervals and longitudinal (coronal) sections of the remainder of the body also at 4 mm intervals. The resolution of the MR images is 256 pixels by 256 pixels. Each pixel has 12 bits of grey tone. We initially analyzed four axial head slices (MRI slice number 1104, 1124, 1134 1154; the first available MRI slice was numbered as 1014) and two coronal thorax slices (Slice # 4450, 4502). The quantitative evaluation values for MRI_1154 and MRI_4450 were shown in Table 10 and 11 but no images from these two slices were presented in this paper because of limited space.

3.1 Experimental design

Both iteration procedures of *a*DWTi-IQI and *a*DWTi-rSFe were implemented by separately varying two parameters, i.e., first changing L_d (because this parameter dominates the fused image quality) then changing L_w to optimize the respective metric. The convergence speed of the *a*DWTi-rSFe is faster than that of the *a*DWTi-IQI. The averaged numbers of iterations for two algorithms are 6 and 13, respectively. The optimized parameters (L_d, L_w) were given in Tables 2-11.

Each MRI slice consists of three bands of images (i.e., a MRI triplet) that are PD-, T1- and T2-weighted images. We applied two algorithms, *a*DWTi-IQI and *a*DWTi-rSFe , to each MRI triplet. Combining any two of three image for each triplet resulted three versions of "two-in-one" (shorted as "2In1") fusions that are PD+T1, PD+T2 and T1+T2. For a "three-in-one" (referred as "3In1") fusion, it seems to be reasonable to fuse three weighted image in one fusion process. However, from the point of view of a realistic application, it is more feasible and practical to fuse two images per fusion process (referred as "two-per-fusion"). For example, after finishing the a MRI triplet fusion, later merging a CT image into the fused MRI image may be desired, then with the two-per-fusion strategy we just need to fuse the fused 3In1-MRI

Table 10: Quantitative evaluations of the fused images (MRI_1154 & 4450) using the *a*DWTi-IQI algorithm

Fusion\Metric	MRI_1154					MRI_4450				
	(L_d,L_w)	IQI	rSFe	**SF**	Entropy	(L_d,L_w)	IQI	rSFe	**SF**	Entropy
PD+T1	(1, 5)	0.9392	-0.1664	27.1856	5.8104	(1, 4)	0.9464	-0.1013	28.3083	6.9059
PD+T2	(2, 7)	0.9475	-0.0443	29.0463	5.8452	(1, 8)	0.9262	-0.0988	23.6172	6.5039
T1+T2	**(1, 2)**	**0.8724**	**-0.0828**	**30.2264**	**5.9976**	**(4, 4)**	**0.8649**	**-0.0124**	**31.8474**	**6.8831**
(PD+T1) +T2	(1, 8)	0.9236	-0.0741	29.8082	5.7863	**(4, 4)**	**0.8850**	**-0.0172**	**30.2017**	**6.6948**
(PD+T2) +T1	(1, 3)	0.9131	-0.1825	28.2942	5.7088	(1, 9)	0.9166	-0.1134	28.5344	6.8506
(T1+T2) +PD	**(1, 7)**	**0.9744**	**-0.0922**	**30.4792**	**5.7855**	(1, 3)	0.9595	-0.0887	30.0748	6.8035

Table 11: Quantitative evaluations of the fused images (MRI_1154 & 4450) using the *a*DWTi-rSFe algorithm

Fusion\Metric	MRI_1154					MRI_4450				
	(L_d,L_w)	IQI	rSFe	**SF**	Entropy	(L_d,L_w)	IQI	rSFe	**SF**	Entropy
PD+T1	(6, 2)	0.9249	-0.0252	31.7917	5.7489	(6, 2)	0.9317	-0.0012	31.4634	7.0143
PD+T2	(6, 2)	0.9363	-0.0063	30.2024	5.6166	(4, 2)	0.9175	-0.0106	25.9269	6.5316
T1+T2	**(4, 5)**	**0.8647**	**0.0384**	**34.2226**	**5.9894**	**(4, 2)**	**0.8577**	**-0.0050**	**32.0882**	**6.8875**
(PD+T1) +T2	(4, 3)	0.9086	-0.0040	35.2688	5.7346	(5, 3)	0.8855	-0.0156	32.8446	6.8318
(PD+T2) +T1	(5, 2)	0.9023	-0.0268	34.442	5.6374	**(6, 2)**	**0.8950**	**-0.0066**	**32.9066**	**6.9543**
(T1+T2) +PD	**(5, 2)**	**0.9495**	**-0.0165**	**36.0819**	**5.7502**	(7, 3)	0.9499	-0.0123	32.8364	6.8660

image and the CT image (unnecessary to restart fusing four images). By following the two-per-fusion strategy, there are also three versions of three-in-one fused images for each MRI triplet, which are (PD+T1)+T2, (PD+T2)+T1 and (T1+T2)+PD (where the parentheses stand for the fusion precedence). We will investigate whether any significant difference existed among the three versions of 3In1 fusions.

With two fusion algorithms applied to a MRI triplet, a total of 12 fused images were yielded. The analyzed results of each triplet were exhibited with two tables and eleven images that were presented on one page (see Tab. 2-9 & Fig. 1-12 on 4 pages following the 'CONCLUSIONS' section). Four quantitative metric values along with optimized parameters were shown in two tables (corresponding to two algorithms). For reference, the SF and entropy values of six original MRI triplets are listed in Table 1. The original three-band images, three versions of two-in-one fused images per algorithm, and one selected three-in-one fused image per algorithm are presented on the page.

3.2 Result analyses and discussions

There are four quantitative evaluations are shown in Tables 2-11 but we need to select one metric to measure the image quality across two different algorithms and a dozen of fused images in order to make fair comparisons. The IQI and rSFe were used as optimization metrics in two algorithms and thus they cannot be selected for comparison. The metric of Entropy is not applicable either because it cannot reflect the relationship between the fused image and the input images. For instance, we expect *Entropy*(PD+T1) ≥ Any{*Entropy*(PD), *Entropy*(T1)}. For most of fusion cases, their Entropy values do not obey this inequation whereas their SF values do. Although the SF metric itself cannot *absolutely* measure

Table 12: The descriptive statistics on the measurement of SF: The fused images were from two groups: SF_2In1 and SF_3In1

Algorithm	Img4Fus	Mean (SF_2In1)	Mean (SF_3In1)	N
*a*DWTi-IQI	Total	30.7021	32.2474	18
***a*DWTi-rSFe**	**Total**	**33.5901**	**36.9068**	**18**
Total	1	32.3638	**34.9485**	12
	2	29.8840	33.8971	12
	3	**34.1905**	34.8857	12

Table 13: The main effects of ANOVA tests on the image quality measures with SF from SF_2In1 and SF_3In1

Fusion Group	Source	df	F	Sig.
SF_2In1 df(Error)=30	**Algorithm**	**1**	**4.313**	**0.046**
	Img4Fus	2	3.221	0.054
	Algo * Img	2	0.181	0.835
SF_3In1 df(Error)=30	**Algorithm**	**1**	**10.308**	**0.003**
	Img4Fus	2	0.22	0.804
	Algo * Img	2	0.112	0.895

the fused image quality because it cannot distinguish useful information from artifacts or noise, it is still suitable to compare fused images' quality (i.e. as a *relative* measurement).

Table 14: The frequency analysis of parameters (L_d, L_w). The "[,]" gives a range of parameter values and the percentage means the normalized frequency.

Statistics	*a*DWTi-IQI		*a*DWTi-rSFe	
	L_d	L_w	L_d	L_w
Mean	1.8	5.7	5.8	2.5
Mode (Percent)	1 (80%)	[3,9] (94%)	[5,7] (89%)	[2,3] (92%)

In each table, one row of three fusions from each fusion group (2In1 or 3In1) was highlighted (corresponding to the largest SF value) according to the SF metric. One of three versions of three-in-one fused images per algorithm was selected to be presented if its SF value is the largest among three of them. From casual observations of illustrated images, the observed results seem to agree with the quantitatively evaluated results. Specifically, both quantitative (by SF) and qualitative (by observation) evaluations (for both algorithms) support that, among 2In1 fusions the fused image "T1+T2" contains the most structural information whereas among 3In1 fusions the fused image "(PD+T1)+T2" is the most informative one. By examining all fused images produced from two algorithms, we found that the fused images using *a*DWTi-IQI are smoothed but the fused images using *a*DWTi-rSFe are sharpened.

In order to determine if the fusion results from the two algorithms and from the three versions of fusions (referred as "Image-for-Fusion" or 'Img4Fus') for each fusion group were significantly different, a 2×3 (i.e., *algorithm* by *image-for-fusion*) two-way repeated measures Analysis of Variance (ANOVA) was carried out on the "SF values" of fused images for each fusion group (2In1 or 3In1, referred as "fusion-group") using SPSS (Version 14). The results of this analysis were shown in Tables 12-13. Table 12 explains that (1) Algorithm "*a*DWTi-rSFe" produces more informative images (with larger mean SF value) than Algorithm *a*DWTi-IQI, which comply with the conclusion of the *a*DWTi-rSFe yields sharpened fused images (refer to the top two rows of Table 12); (2) in the fusion group of '2In1', the fused image "T1+T2" (labeled as '3') has the largest mean SF (= 34.1905) whereas in fusion-group 3In1 the mean SF of "(PD+T1)+T2" (labeled as '1') is the biggest (= 34.9485) (the bottom three rows of Table 12). From Table 13, we learn that for both 2In1 and 3In1 fusion groups, the main effect on factor "Algorithm" is significant ($p = 0.046$ and 0.003) but no significance is shown for factor "Img4Fus" ($p = 0.054$ and 0.804), and non-significant interaction is found between these two factors. Based on the statistical results (in Table 13), we can conclude that Algorithm *a*DWTi-rSFe is superior to *a*DWTi-IQI (in the sense of SF metric), non-significant difference among three versions of 3in1 fusions is found. However, for three versions of 2in1 fusions, we have $p = 0.054$ that means, strictly speaking, non-significant difference (maybe due to small samples), however, the differences are observable from both quantitative analyses (Table 12) and figure illustrations (Figs. 1-12).

Another interesting question is what the optimization values for parameters (L_d, L_w) are. Although they rely on a particular image the frequency analysis (as shown in Table 14) can show some typical values. For example, to have an optimized fusion by running Algorithm *a*DWTi-rSFe, we may initially set (L_d, L_w) = (6, 3) that will speed up the convergence.

3.3 Future work

We planned to analyze a large sample of images such that more accurate statistical analyses will be conducted. We may apply the two iterative *a*DWTi algorithms to multimodality image fusion (e.g., with CT, PET) and further follow up the fusion benefits on segmentation and colorization.[33]

4. CONCLUSIONS

Two iterative fusion procedures (*a*DWTi-IQI and *a*DWTi-rSFe) are developed and successfully applied to three-band (PD, T1 and T2) MRI image fusion. The fused images were evaluated quantitatively and statistically (and with visual inspections, too). The informative fused images were recommended and two fusion procedures were compared on the basis of image quality evaluation. From the experimental results yielded by the *a*DWTi-IQI and *a*DWTi-rSFe, we found that that (1) the *a*DWTi-IQI algorithm produces a smoothed image whereas the *a*DWTi-rSFe algorithm yields a sharpened image, (2) fused image "T1+T2" is the most informative one in comparison with other two-in-one fusions (PD+T1 and PD+T2), (3) for three-in-one fusions, no significant difference is observed among the three fusions of (PD+T1)+T2, (PD+T2)+T1 and (T1+T2)+PD, thus the order of fusion does not play an important role. The fused images are greatly useful for diagnosis purpose and also significantly benefit the further image processing such as multi-modality image fusion (with CT images), visualization (colorization), segmentation, classification and computer-aided diagnosis (CAD).

Table 2: Quantitative evaluations of the fused images (with MRI_1104) using the *a*DWTi-IQI algorithm (Fig. 2)

Fusion\Metric	(L_d,L_w)	IQI	rSFe	SF	Entropy
PD+T1	(1, 5)	0.9318	-0.1831	27.7975	5.5812
PD+T2	(1, 5)	0.9307	-0.1041	28.2410	5.7780
T1+T2	**(5, 6)**	**0.8655**	**-0.0336**	**31.8010**	**5.6434**
(PD+T1) +T2	**(5, 6)**	**0.9105**	**-0.0213**	**31.5688**	**5.4785**
(PD+T2) +T1	(1, 7)	0.9135	-0.1619	28.8772	5.4872
(T1+T2) +PD	(1, 3)	0.9526	-0.1214	31.5619	5.6508

Table 3: Quantitative evaluations of the fused images (with MRI_1104) using the *a*DWTi-rSFe algorithm (Fig. 3)

Fusion\Metric	(L_d,L_w)	IQI	rSFe	SF	Entropy
PD+T1	**(6, 2)**	**0.9220**	**-0.0309**	**32.9776**	**5.6725**
PD+T2	(7, 2)	0.9226	-0.0090	31.2410	5.2386
T1+T2	(7, 2)	0.8609	-0.0119	32.5138	5.3378
(PD+T1) +T2	(7, 3)	0.9054	-0.0218	35.2481	5.4090
(PD+T2) +T1	(7, 2)	0.9080	-0.0294	35.1693	5.3829
(T1+T2) +PD	**(5, 3)**	**0.9435**	**-0.0329**	**35.3353**	**5.5739**

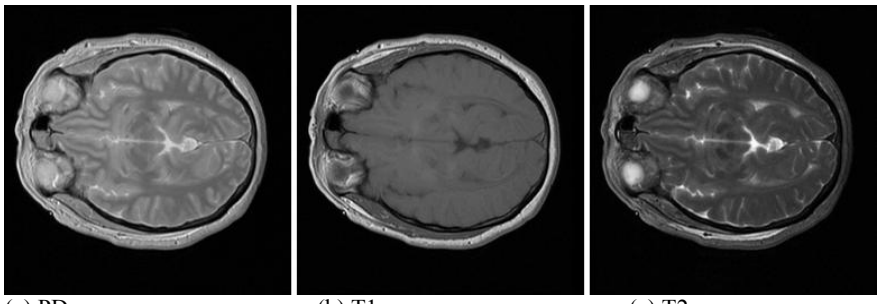

(a) PD (b) T1 (c) T2

Figure 1: The MRI triplet of a head slice (from the Visible Human Project® female data): MRI_1104

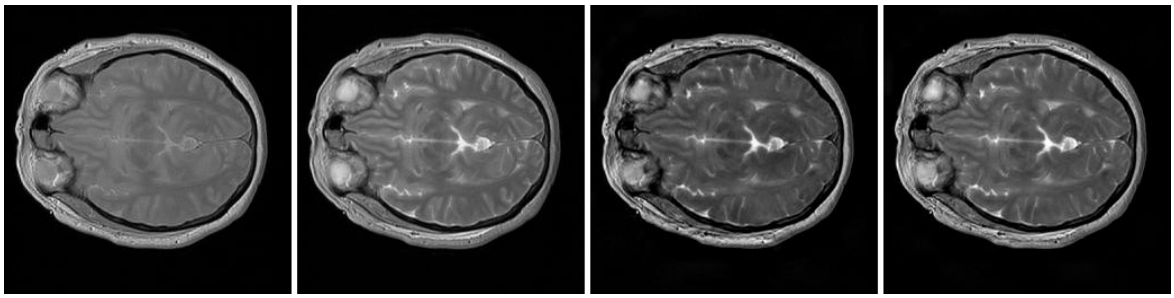

(a) PD+T1 (b) PD+T2 (c) **T1+T2** (d) (PD+T1) +T2

Figure 2: The fused images (with MRI_1104) using the *a*DWTi-IQI algorithm

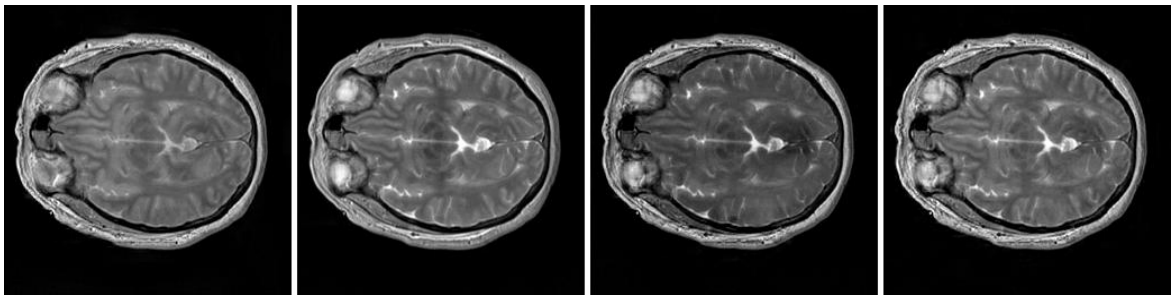

(a) **PD+T1** (b) PD+T2 (c) T1+T2 (d) (T1+T2)+PD

Figure 3: The fused images (with MRI_1104) using the *a*DWTi-rSFe algorithm

Table 4: Quantitative evaluations of the fused images (with MRI_1124) using the *a*DWTi-IQI algorithm (Fig. 5)

Fusion\Metric	(L_d,L_w)	IQI	rSFe	SF	Entropy
PD+T1	**(1, 3)**	**0.9320**	**-0.1395**	**29.9470**	**5.6500**
PD+T2	(1, 8)	0.9413	-0.1018	29.1358	5.7777
T1+T2	(1, 10)	0.8566	-0.1454	29.6918	5.7427
(PD+T1) +T2	**(1, 6)**	**0.9155**	**-0.0909**	**31.5028**	**5.6611**
(PD+T2) +T1	(1, 7)	0.9123	-0.1558	30.0149	5.5341
(T1+T2) +PD	(1, 7)	0.9733	-0.1023	30.6811	5.6437

Table 5: Quantitative evaluations of the fused images (with MRI_1124) using the *a*DWTi-rSFe algorithm (Fig. 6)

Fusion\Metric	(L_d,L_w)	IQI	rSFe	SF	Entropy
PD+T1	(5, 2)	0.9207	-0.0270	33.8631	5.6621
PD+T2	(6, 2)	0.9311	-0.0136	31.9975	5.5164
T1+T2	**(7, 2)**	**0.8400**	**-0.0135**	**34.2741**	**5.5141**
(PD+T1) +T2	(7, 3)	0.9005	-0.0254	36.5365	5.4126
(PD+T2) +T1	(6, 2)	0.8911	-0.0297	36.2728	5.4791
(T1+T2) +PD	**(5, 3)**	**0.9439**	**-0.0280**	**36.8215**	**5.6574**

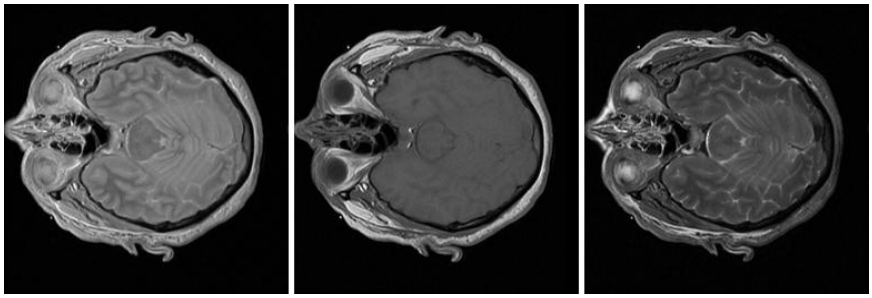

(a) PD (b) T1 (c) T2

Figure 4: The MRI triplet of a head slice (from the Visible Human Project® female data): MRI_1124

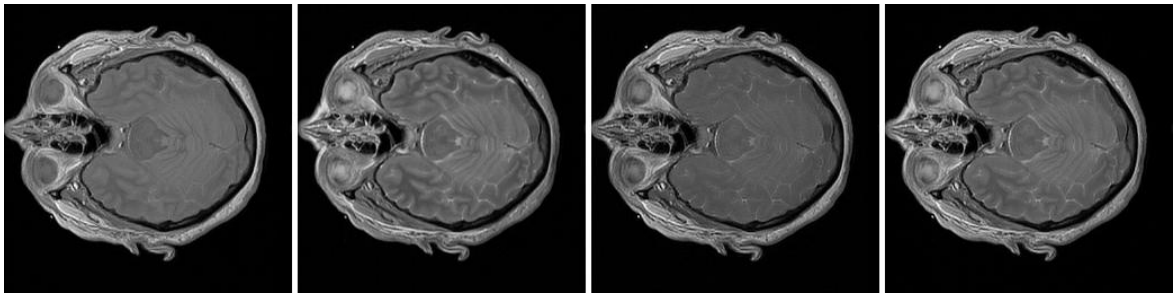

(a) **PD+T1** (b) PD+T2 (c) T1+T2 (d) (PD+T1) +T2

Figure 5: The fused images (with MRI_1124) using the *a*DWTi-IQI algorithm

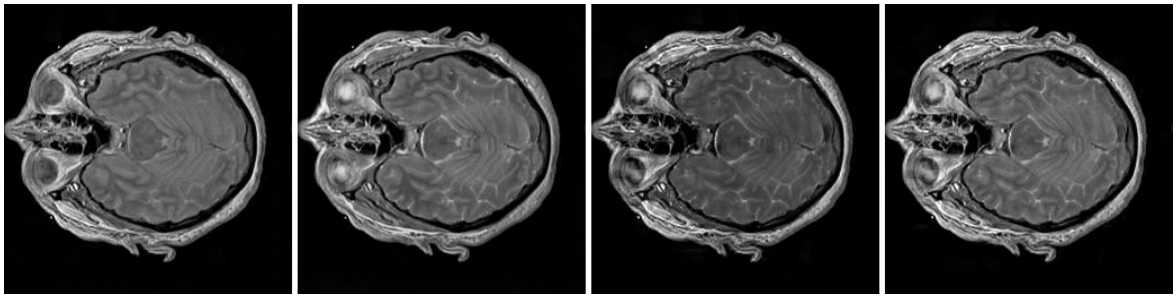

(a) PD+T1 (b) PD+T2 (c) **T1+T2** (d) (T1+T2)+PD

Figure 6: The fused images (with MRI_1124) using the *a*DWTi-rSFe algorithm

Table 6: Quantitative evaluations of the fused images (with MRI_1134) using the *a*DWTi-IQI algorithm (Fig. 8)

Fusion\Metric	(L_d,L_w)	IQI	rSFe	SF	Entropy
PD+T1	(1, 7)	0.9310	-0.1461	30.4919	5.8607
PD+T2	(1, 3)	0.9371	-0.1128	26.1649	5.6048
T1+T2	**(1, 9)**	**0.8591**	**-0.0846**	**32.5301**	**5.9368**
(PD+T1) +T2	(1, 9)	0.9001	-0.0773	31.6277	5.6585
(PD+T2) +T1	(1, 3)	0.9030	-0.1194	31.5931	5.7268
(T1+T2) +PD	**(1, 7)**	**0.9649**	**-0.1051**	**31.9018**	**5.7173**

Table 7: Quantitative evaluations of the fused images (with MRI_1134) using the *a*DWTi-rSFe algorithm (Fig. 9)

Fusion\Metric	(L_d,L_w)	IQI	rSFe	SF	Entropy
PD+T1	(5, 3)	0.9133	-0.0299	34.6410	5.7268
PD+T2	(5, 3)	0.9283	-0.0117	29.1458	5.4762
T1+T2	**(7, 2)**	**0.8480**	**-0.0163**	**34.9580**	**5.3328**
(PD+T1) +T2	**(7, 2)**	**0.8894**	**-0.0160**	**36.7621**	**5.0196**
(PD+T2) +T1	(5, 3)	0.8811	-0.0334	36.2251	5.5784
(T1+T2) +PD	(5, 3)	0.9374	-0.0301	36.6863	5.4615

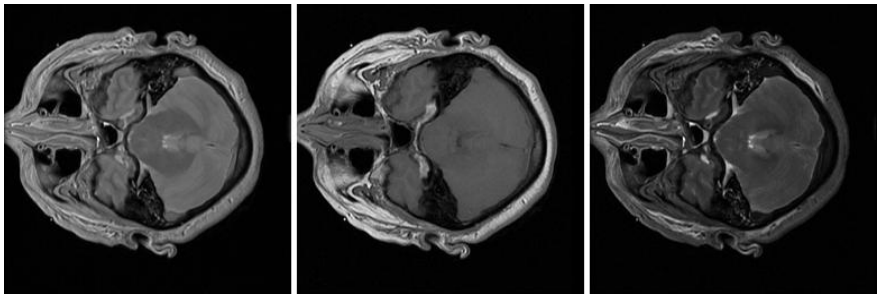

(a) PD (b) T1 (c) T2

Figure 7: The MRI triplet of a head slice (from the Visible Human Project® female data): MRI_1134

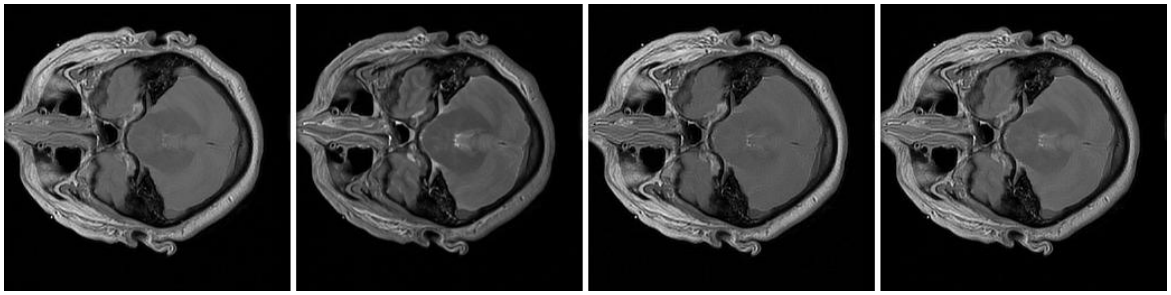

(a) PD+T1 (b) PD+T2 (c) **T1+T2** (d) (T1+T2)+PD

Figure 8: The fused images (with MRI_1134) using the *a*DWTi-IQI algorithm

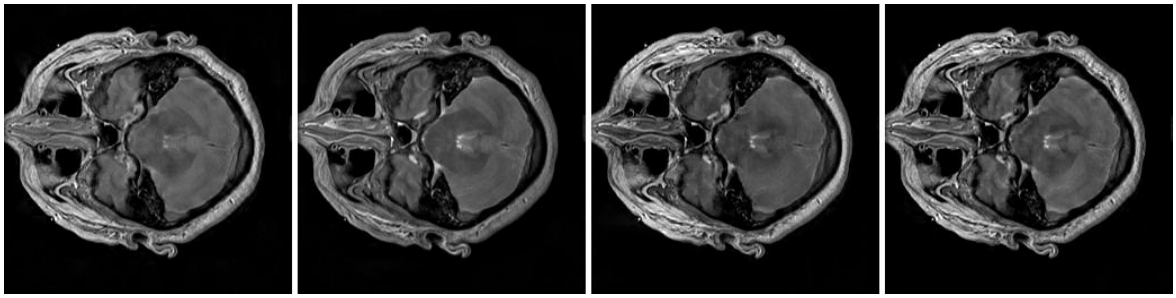

(a) PD+T1 (b) PD+T2 (c) **T1+T2** (d) (PD+T1)+T2

Figure 9: The fused images (with MRI_1134) using the *a*DWTi-rSFe algorithm

Table 8: Quantitative evaluations of the fused images (with MRI_4502) using the *a*DWTi-IQI algorithm (Fig. 11)

Fusion\Metric	(L_d,L_w)	IQI	rSFe	SF	Entropy
PD+T1	(1, 7)	0.9476	-0.0743	38.4339	7.2207
PD+T2	(1, 9)	0.9191	-0.0950	35.1055	7.0522
T1+T2	**(7, 4)**	**0.8404**	**-0.0072**	**43.0664**	**7.0923**
(PD+T1) +T2	**(7, 4)**	**0.8795**	**-0.0058**	**43.1187**	**7.0421**
(PD+T2) +T1	(1, 4)	0.9105	-0.0925	39.3016	7.1604
(T1+T2) +PD	(1, 3)	0.9557	-0.0839	41.3109	7.1802

Table 9: Quantitative evaluations of the fused images (with MRI_4502) using the *a*DWTi-rSFe algorithm (Fig. 12)

Fusion\Metric	(L_d,L_w)	IQI	rSFe	SF	Entropy
PD+T1	(6, 2)	0.9286	-0.0013	41.4649	7.2219
PD+T2	(6, 2)	0.9084	-0.0002	38.7840	6.9958
T1+T2	**(7, 4)**	**0.8404**	**-0.0072**	**43.0664**	**7.0923**
(PD+T1) +T2	(7, 3)	0.8781	-0.0124	44.8934	7.0974
(PD+T2) +T1	**(5, 4)**	**0.8911**	**-0.0049**	**45.1335**	**7.1698**
(T1+T2) +PD	(6, 2)	0.9451	-0.0052	44.8578	7.3281

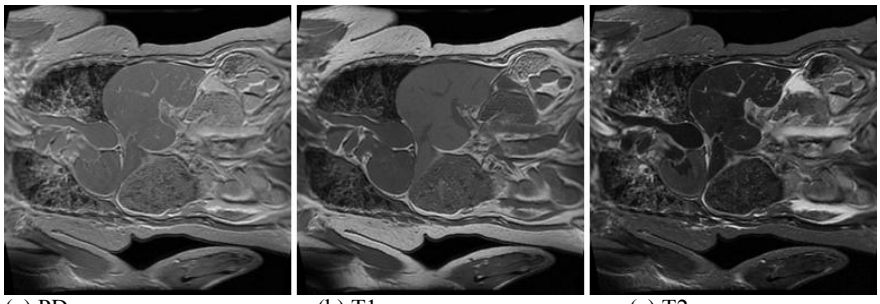

(a) PD (b) T1 (c) T2

Figure 10: The MRI triplet of a thorax coronal slice (from the Visible Human Project® female data): MRI_4502

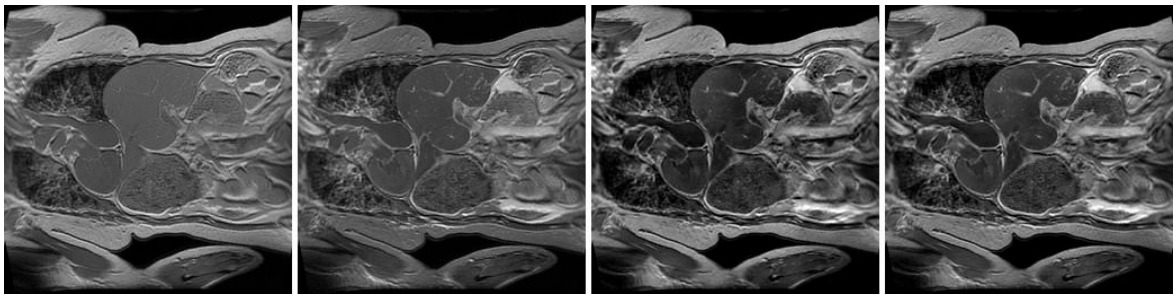

(a) PD+T1 (b) PD+T2 (c) **T1+T2** (d) (PD+T1) +T2

Figure 11: The fused images (with MRI_4502) using the *a*DWTi-IQI algorithm

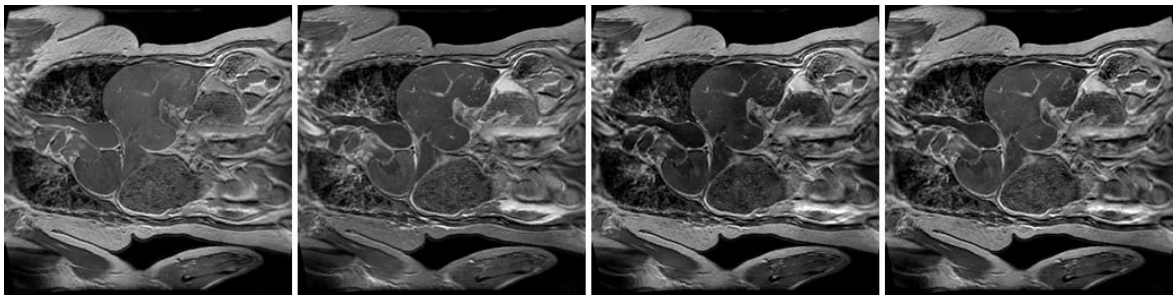

(a) PD+T1 (b) PD+T2 (c) **T1+T2** (d) (PD+T2) +T1

Figure 12: The fused images (with MRI_4502) using the *a*DWTi-rSFe algorithm

REFERENCES

1. L. D. Keys, N. J. Schmidt, and B. E. Phillips, A prototype example of sensor fusion used for a siting analysis, in Technical Papers 1990, ACSM-ASPRS Annual Conv. Image Processing and Remote Sensing 4, pp. 238–249 (1990).
2. R. H. Rogers and L. Wood, The history and status of merging multiple sensor data: an overview, in Technical Papers 1990, ACSMASPRS Annual Conv. Image Processing and Remote Sensing 4, pp. 352–360 (1990).
3. E. A. Essock, M. J. Sinai, J. S. McCarley, W. K. Krebs, and J. K. DeFord, Perceptual ability with real-world nighttime scenes: imageintensified, infrared, and fused-color imagery, Hum. Factors 41(3), 438–452 (1999).
4. E. A. Essock, J. S. McCarley, M. J. Sinai, and J. K. DeFord, Human perception of sensor-fused imagery, in Interpreting Remote Sensing Imagery: Human Factors, R. R. Hoffman and A. B. Markman, Eds., Lewis Publishers, Boca Raton, Florida (Feb. 2001).
5. C. Pohl and J. L. Van Genderen, Review article: multisensor image fusion in remote sensing: concepts, methods and applications, Int. J. Remote Sens. 19(5), 823–854 (1998).
6. O. Rockinger, Pixel level fusion of image sequences using wavelet frames, in Proc. 16th Leeds Applied Shape Research Workshop, pp. 149–154, Leeds University Press (1996).
7. H. Li, B. S. Manjunath, and S. K. Mitra, Multisensor image fusion using the wavelet transform, Graph. Models Image Process. 57(3), 235–245 (1995).
8. T. Pu and G. Ni, Contrast-based image fusion using the discrete wavelet transform, Opt. Eng. 39(8), 2075–2082 (2000).
9. D. A. Yocky, Image merging and data fusion by means of the discrete two-dimensional wavelet transform, J. Opt. Soc. Am. A 12(9), 1834–1841 (1995).
10. J. Nunez, X. Otazu, O. Fors, A. Prades, V. Pala, and R. Arbiol, Image fusion with additive multiresolution wavelet decomposition; applications to spot1landsat images, J. Opt. Soc. Am. A 16, 467–474 (1999).
11. F. Jahard, D. A. Fish, A. A. Rio, and C. P. Thompson, Far/near infrared adapted pyramid-based fusion for automotive night vision, in IEEE Proc. 6th Int. Conf. on Image Processing and its Applications (IPA97), pp. 886–890 (1997).
12. B. Ajazzi, L. Alparone, S. Baronti, and R. Carla, Assessment of pyramid-based multisensor image data fusion, in Proc. SPIE 3500, 237–248 (1998).
13. P. J. Burt, The pyramid as structure for efficient computation, in Multiresolution Image Processing and Analysis, A. Rosenfeld, Ed., pp. 6–35, Springer-Verlag, New York/Berlin (1984).
14. P. J. Burt and E. Adelson, The Laplacian pyramid as a compact image code, IEEE Trans. Commun. Com-31(4), 532–540 (1983).
15. A. Toet, Image fusion by a ratio of low pass pyramid, Pattern Recogn. Lett. 9(4), 245–253 (1989).
16. A. Toet, L. J. Van Ruyven, and J. M. Valeton, Merging thermal and visual images by contrast pyramid, Opt. Eng. 28(7), 789–792 (1989).
17. A. Toet, Hierarchical image fusion, Mach. Vision Appl. 3(1), 1–11 (1990).
18. P. J. Burt, A gradient pyramid basis for pattern-selective image fusion, SID Int. Symp. Digest Tech. Papers 16, 467–470 (1985).
19. A. Toet, A morphological pyramid image decomposition, Pattern Recogn. Lett. 9(4), 255–261 (1989).
20. G. K. Matsopoulos, S. Marshall, and J. Brunt, Multiresolution morphological fusion of MR and CT images of the human brain, IEE Proc. Vision Image Signal Process. 141(3), 137–142 (1994).
21. G. K. Matsopoulos and S. Marshall, Application of morphological pyramids: fusion of MR and CT phantoms, J. Visual Commun. Image Represent 6(2), 196–207 (1995).
22. Y. Zheng, E. A. Essock, and B. C. Hansen, An advanced image fusion algorithm based on wavelet transform—incorporation with PCA and morphological processing, Proc. SPIE 5298, 177–187 (2004).
23. Y. Zheng, E. A. Essock, and B. C. Hansen, An advanced DWT fusion algorithm and its optimization by using the metric of image quality index, Optical Engineering, 44(3), 037003-1-12 (2005).
24. Y. Zheng, E. A. Essock, and B. C. Hansen and A. M. Haun, A new metric based on extended spatial frequency and its application to DWT based fusion algorithms, Information Fusion, (In Press).
25. M. Aguilar, A. L. Garrett, Biologically based sensor fusion for medical imaging, Proc. SPIE Vol. 4385, pp. 149-158, Sensor Fusion: Architectures, Algorithms, and Applications V, B. V. Dasarathy; Ed (2001).
26. M. Aguilar and J. R. New, Fusion of Multi-Modality Volumetric Medical Imagery, Proceedings of the Fifth International Conference on Information Fusion (2002), Annapolis, MD.
27. P. J. Burt and E. H. Adelson, Merging images through pattern decomposition, Proc. SPIE 575, 173–182 (1985).
28. Z. Wang and A. C. Bovik, A universal image quality index, IEEE Signal Process. Lett. 9(3), 81–84 (2002).
29. G. Piella and H. Heijmans, A new quality metric for image fusion, in Proc. 2003 Int. Conf. on Image Processing, Barcelona, Spain (2003).
30. A. M. Eskicioglu and P. S. Fisher, Image quality measure and their performance, IEEE Trans. Commun. 43(12), 2959–2965 (1995).
31. S. Li, J. T. Kwok, and Y. Wang, Combination of images with diverse focuses using the spatial frequency, Infusionstherapie 2(3), 169–176 (2001).
32. R. C. Gonzalez and R. E. Woods, Digital Image Processing, 2nd ed., Prentice Hall, Upper Saddle River, NJ (2002).
33. Y. Zheng, B. C. Hansen and A. M. Haun and E. A. Essock, Coloring Night-vision Imagery with Statistical Properties of Natural Colors by Using Image Segmentation and Histogram Matching, Proceedings of the SPIE, Vol. 5667, pp. 107-117 (2005).